

www.acsami.org Research Article

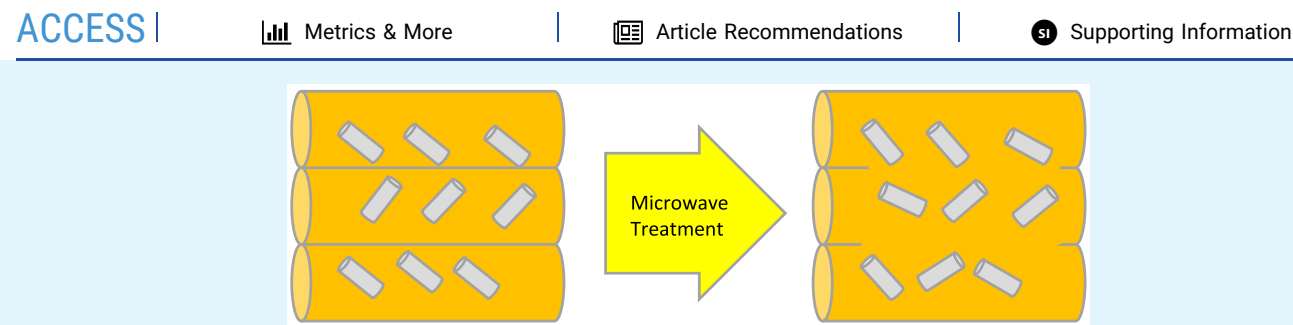
Enhancement of Polypropylene 3D-Printed Structures via the Addition of SiC Whiskers and Microwave Irradiation

Erik L. S. Antonio, Arefin M. Anik, Olga Kuksenok,* and Igor Luzinov*



Cite This: ACS Appl. Mater. Interfaces 2023, 15, 40042–40053





ABSTRACT: We report on enhancing the mechanical and structural characteristics of polypropylene (PP) three-dimensional (3D)-printed structures fabricated via fused filament fabrication (FFF) by employing composite PP-based filament with subsequent microwave (MWV) treatment. The composite filament contained a minute (0.9 vol %) fraction of silicon carbide whiskers (SiCWs) and was prepared via melt blending of PP pellets with SiCW using an extruder. The surface of the whiskers was modified with trimethoxy(octadecyl) silane to improve compatibility between the polar SiCW and nonpolar PP matrix. We employed SiCWs in composite filament because of the whiskers' high thermal conductivity and ability to generate heat locally under MWV irradiation. Indeed, we were able to conduct the heating of printed parts by MWV without sacrificing the structural integrity and improving the overall adhesion between the 3D-printed polymer layers. Our modeling captures an extent of heating upon MWV irradiation observed in our experiments. In general, utilization of the composite PP/SiCW filament significantly improved the printed parts' mechanical characteristics and sintering level compared to those made from pure PP filament. Specifically, after the MWV treatment, the adjusted (for density) storage modulus of the PP/SiCW material was just ~20% lower than that for the PP sample obtained by conventional compression molding. After the MWV irradiation, Young's modulus, yield stress, and toughness of the printed structures were increased by ~65, 53, and 55%, respectively. We attribute the improvement of mechanical properties via MWV treatment to enhancing the entanglement level at the weld.

KEYWORDS: polypropylene, 3D printing, mechanical properties, microwave irradiation, silicon carbide whiskers

■ INTRODUCTION

The field of three-dimensional (3D) printing, commonly referred to as additive manufacturing (AM) or rapid prototyping (RP) earlier, was first developed by Charles Hull in the 1980s based on his work with photopolymerization. In the field has exploded, often called the "new industrial revolution". One of the most widely used methods of polymer-based 3D printing is fused deposition modeling (FDM) or fused filament fabrication (FFF), which requires a thermoplastic filament to be directed toward a heating block and then deposited via extrusion layer-by-layer to produce a finished part. Generally, FFF-printed parts have lower strength, toughness, and reliability than parts produced through traditional methods, such as injection and compressive molding. Also, due to the nature of FFF, 3D-printed parts can demonstrate anisotropic behavior with varying properties depending on the orientation of applied stress.

Currently, the most pressing FFF challenge is the limited selection of materials that can be used in this technique, as the

process requires that a filament has a viscosity high enough to provide structural support but low enough for proper extrusion mechanical consolidation. For instance, polypropylene (PP) is one of the world's most widely used thermoplastic polymers, known for its mechanical properties, processibility, chemical resistance, and low cost. Due to its widespread use, ample interest is in implementing the polymer in FFF. However, like other semicrystalline polymers crystallizing at a high rate, the 3D printing of PP faces significant obstacles. The challenges are mainly due to the fast cooling in the FFF printing process, which leads to significant volume shrinkage and limited interdiffusion (consolidation) at the printed layer interface as

Received: May 24, 2023 Accepted: July 26, 2023 Published: August 8, 2023





Figure 1. Scheme for the PP/SiCW layer welding via the MWV treatment process.

rapid crystallization occurs. ^{11–13} In addition, the crystallization process can differ within a printed part due to print patterns, part dimensions, and printing speed variation. ¹⁴

To this end, this work focuses on improving the properties of PP 3D-printed structures by employing composite PP-based filament containing a minute (3 wt % or 0.9 vol %) fraction of silicon carbide whiskers (SiCWs). Previously, adding inorganic fillers to filaments used in FFF has been shown to reinforce the polymeric material, reduce shrinkage from printing, and decrease the anisotropy of printed parts. The addition of inorganic fillers appears as a possible solution to close the gap between FFF-produced parts and traditional fabrication methods, provided that concentration and the interfacial interaction between the inorganic filler and polymer matrix are adequately addressed. 16,17

The attractiveness of employing SiCWs in composite materials resides in their exceptional physical properties, such as a high modulus, thermal and radiation stability, abrasion resistance, a low coefficient of thermal expansion, high thermal conductivity, and low electrical conductivity. 18-21 Further, SiCWs are fabricated from rice hulls, a renewable material.²² The surface of SiCWs contains SiO₂ groups²² and, therefore, can be straightforwardly modified using silane chemistry^{21,23} to be compatible with nonpolar polymer materials such as PP. The whiskers were also chosen due to their ability to absorb microwave (MWV) irradiation and generate heat locally.^{24,25} Using such materials combined with polymer matrices is very appealing, as MWV heat treatment can be used for postprocessing purposes such as joining and/or repairing damaged interfaces. 25,26 We envisioned allowing local heating of the already printed parts without sacrificing the structural integrity and improving the overall adhesion between the 3Dprinted polymer layers (Figure 1). Prior FFF studies utilizing different microwave-absorbing materials/polymer pairs such as ABS/carbon nanotubes (CNTs),²⁷ PLA (polylactic acid)/ CNT,²⁸ PLA/SiC,²⁹ and PLA/graphene³⁰ demonstrated the efficiency of this approach. It is worth mentioning that ABSand PLA FFF-printed structures (even without MWV treatment) have good mechanical properties, are easy to print, and are widely employed in FFF. However, to the best of our knowledge, this methodology has not been applied to improve 3D-printed structures made from the "difficult-toprint" PP.

We found that employing the composite PP/SiCW filament in the FFF process improved the printed parts' structural and mechanical characteristics compared to those made from pure PP filament. In addition, introducing the whiskers in the material offered measurable temperature increases in printed composite parts during subsequent microwave treatment. This further treatment did not change the part dimensions/shape and offered additional time for the polymer chain rearrangement/entanglement at the interface between printed layers.

We demonstrated that the MWV irradiation significantly improved the mechanical properties of the 3D-printed materials.

EXPERIMENTAL SECTION

Materials. Polypropylene (1.3 MFI Braskem F013M) pellets were used as received. Methyl ether ketone (MEK) was purchased from Sigma-Aldrich. Silar SC-9M SiCWs were obtained from Advanced Composite Materials LLC. SiCWs were rinsed 3 times with MEK before use. Trimethoxy(octadecyl)silane (TOS) was obtained from Alfa Aesar. As reported previously, 21 the obtained whiskers have diameters in the range of 0.2–0.6 μ m (0.42 μ m average) and lengths from 2 to16 μ m (4.2 μ m average).

Modification of SiCWs. First, a 5% volume TOS solution was prepared by adding the silane to MEK. SiCWs were added to the solution, and the suspension was agitated overnight on an orbital shaker set to a low speed. The modified SiCWs were separated from the solution via sedimentation, rinsed 3 times with MEK to remove unbonded TOS, and dried at ambient conditions for at least 24 h. The amount of TOS attached was determined via mass loss using Thermal Gravitation Analysis (TGA Q5000, TA Instruments). In the TGA experiments, a sample (~5 mg) was heated under a nitrogen atmosphere (gas flow = 20 mL/min) from 25 to 700 °C at a heating rate of 20 °C/min. The thickness of the TOS layer was calculated from the mass loss as described elsewhere.²¹

Preparation of PP and PP/SiCW Filaments. A Noztek single screw extruder (equipped with a spool winder control system) having a 1.75 mm die was used at 230 °C to extrude filaments from PP and PP/SiCW pellets. We extruded the filament twice to prepare the PP/ SiCW material. The double extrusion with the single screw extruder was needed to obtain the samples with even distribution of SiCWs within the PP filament. Since the double extrusion at the elevated temperature can change the material properties, the pure PP filament was also produced using the same procedure employed for the PP/ SiCW filament. To fabricate the PP/SiCW filament, 50 g of PP pellets was placed in a 300 mL glass beaker. The MEK/SiCW suspension was then slowly dropped over the pellets in a drop-casting-like nature until the solution was exhausted, and the pellets were thoroughly coated. During the drop-casting, the pellets were manually mixed using a spatula. The pellets decorated with SCWs were placed in a Petri dish, loosely covered with aluminum foil, and dried thoroughly for 24-48 h to allow the MEK solvent to evaporate. The drying was completed when the MEK smell was not detected organoleptically. The composite filament was prepared by placing SiCW-coated pellets in the hopper for 15 min for preheating before initial extrusion. The extruded filament was chopped up and fed back into the extruder for a second extrusion.

Preparation of 3D-Printed Materials. Samples were printed on a Builder 3D FDM Printer for DMA and compressive testing. The dimensions of the DMA samples were $35 \times 7 \times 2$ mm³. The samples for compression testing were $10 \times 10 \times 10$ mm³ cubes. In order to accurately measure the temperature of our materials, a variation of the compression cubes was printed with a 5 mm deep hole (diameter 2 mm) added to allow for our fiber optic temperature probe. Designs were made on Solidworks software, and printing parameters were finalized on Slic3r software with a 0.4 mm layer height, a 100% infill, a 60 mm/s parameter speed, an 80 mm/s infill speed, and a 130 mm/s

travel speed. All samples were printed at 230 $^{\circ}$ C onto a 40 $^{\circ}$ C heated bed. The printing direction was $\pm 45^{\circ}$. A PP thin film was used to improve bed adhesion during printing.

Density of the 3D-Printed Materials. The samples' dimensions and weight were measured to determine the density of the materials printed. The dimensions (at multiple points) were measured using a micrometer. The weight was determined with an analytical balance. In the calculations, we used the average value of the dimensions, and the samples were considered to have a rectangular shape.

Microwave Irradiation. Microwave treatment was performed on a 1000 Watt Laboratory Microwave BP-095 from Microwave Research and Applications Inc. The samples (enclosed in the thermoinsulating PP foam container) were positioned in the middle of the microwave in the plane (X-Y) direction and \sim 5 cm in the vertical (Z) direction. The temperature of the microwave oven chamber and the cube was measured using a FOTEMP1-H single-channel portable signal conditioner equipped with a fiber optics FO, type TS3 temperature probe (Micronor Sensors).

Characterization. Hitachi SEM 4800 and SEM 6600 scanning electron microscopes were utilized to examine the filament cross sections. Filament cross-sectional samples were prepared via cryogenic fracture. To this end, the filament samples (about 3 cm long) were employed. A notch (~1 mm deep) was made with a razor blade in the middle of the filament. Next, the samples were placed into liquid nitrogen for 10 min. Finally, the samples were broken using two pliers. Differential scanning calorimetry (DSC) was used to evaluate the thermal properties. The measurements were conducted at a 20 °C/ min rate between -50 and 200 °C. Dynamic mechanical analysis (DMA, Q800 TA Instruments) was used to characterize thermalmechanical properties. The temperature was ramped from -50 to 120 °C with a rate of 2 °C per min and a frequency of 5.0 Hz. For compression testing, $10 \times 10 \times 10 \text{ mm}^3$ -printed cubes were used. The testing was done on an Instron 2282 at a 10 mm/min compression rate. Three parallel DMA and compression samples were tested per each material.

RESULTS AND DISCUSSION

Evaluation of Interfacial Situation. It is well established that due to the nature of FFF printing, mechanically weak points occur along the contact line between the extruded layers. 16,31-33 The strength of the link between the two polymer surfaces welded together is directly tied to the degree of interdiffusion at the boundary. 34-36 The contracting polymer chains must diffuse and create a welded zone between the two surfaces whose strength depends on the level of entanglements that can form. The polymer chains must diffuse a distance of approx. 0.4 R_g , where R_g is the macromolecule's gyration radius, to regain the bulk strength³⁶ and attain interfacial healing during printing. The extent of the interdiffusion during the 3D printing is defined by the temperature profile within the printed layer, with the local diffusion coefficient dependent on the instantaneous temperature. We approximate the temperature T within the printed layer during the printing process as

$$T = T_{\rm C} + (T_{\rm m} - T_{\rm C}) \frac{\Delta h}{\sqrt{\pi \varphi t}} \exp\left(-\frac{Z^2}{4\varphi t}\right)$$
 (1)

where T_c is the chamber temperature (K), T_m is the temperature of the newly deposited layer (K), Δh is the layer thickness (m), ϕ is the thermal diffusivity (m/s²), t is time (s), and Z is the vertical coordinate within the layer (m).

The temperature profile for the PP printing conducted in this work (estimated by eq 1) is shown in the Supporting Information, SI (S1 and Figure S1). The importance of the cooling profile is twofold. First, polymer mobility is directly tied to the system's temperature through its relationship with

diffusion. Second, polymer chains can only diffuse significantly above certain key temperatures: glass-transition temperature (T_g) for the amorphous phase and crystallization temperature (T_{cr}) for the crystalline phase. For PP used here, T_{g} determined from DMA of the compression-molded sample is about −5 °C (SI: S6 and Figure S5); however, the chain mobility is severely limited once rapid crystallization is completed at ~110 °C (SI: S7 and Figure S6). From the cooling profile (SI: Figure 1S), we concluded that PP chains reach a stopping point in their long-range diffusion after approx. 3 s as T_{cr} is attained. From the PP molecular weight (M_W~412,000 g/mol, SI: S2) and literature data on the PP self-diffusion coefficient (SI: S3), we obtained an equation that allowed us to find the diffusion coefficient across broad temperature ranges for PP material used here (SI: S3 and eq S3). The relationship between temperature and diffusion coefficient was combined with the cooling curve data (Figure S3) to estimate the change in the macromolecule diffusivity as the system cooled. We found that the PP chains are capable of traveling about \sim 14 nm, while the estimated R_g for the chains is approx. 20 nm (SI, S3 and S4). Thus, the required distance for healing the PP/PP interface in the course of printing is about 8 nm $(0.4 \times R_{\sigma})$.

The estimations above show sufficient time for the full interfacial healing of PP/PP boundaries when printed at 230 °C. Thus, the strength of the welds between the printed layers had to reach a maximum value. However, it was reported that interdiffusion and entanglement of the melt across the interface are significantly affected by high shear rates in the nozzle.³⁸ The shear stress causes deformation and disentanglement of the polymer chains before welding, reducing mechanical strength at the layers' contacts. Specifically, even if a macromolecule diffusion distance is on the level of $R_{\rm g}$, chain orientation/deformation does not fully relax during the welding time. To this end, theoretical calculations indicate the importance of the entanglement number, $Z_{EQ} = M_W/M_E$ $(M_{\rm E}$ is the molecular weight between entanglements).³⁸ The smaller the number, the higher the extent of the chain interpenetration at the layer contact. It was found that at Z_{EO} ≤ 22 the weld thickness becomes independent of the deformation induced by shear rates in the nozzle at any printing speed.³⁸

The weld mechanical strength in the 3D printing process is generally connected to the interdiffusion thickness $S_{\rm thick}$ and the integrity of the entanglement network at the weld, $\nu_{\rm W}$. The bulk strength at the contact is expected for $\nu_{\rm W}=1$ and $S_{\rm thick}/R_{\rm g}>1.^{38}$ In our case, the ratio is about 0.7. The integrity of the entanglement network is a function of $Z_{\rm EQ}$, polymer thermal behavior, and printing parameters. We used the known $M_{\rm E}$ value PP (4620 g/mol)³⁶ to estimate $Z_{\rm EQ}$ as 89. McIlroy and Olmsted³⁸ showed theoretically that under the same printing conditions, $\nu_{\rm W}$ for a polymer having a $Z_{\rm EQ}$ of 40 is 5–10 times larger than $\nu_{\rm W}$ for a polymer with a $Z_{\rm EQ}$ of 80. Thus, we can conclude that in our case, the mechanical strength of the PP-based printed structure cannot rich the highest possible value during printing. Therefore, MWV postheating can potentially improve the mechanical properties of the fabricated printed parts.

Composite Filaments for 3D FFF Printing. Prior studies have shown that polar SiC does not disperse well in the nonpolar polypropylene matrix.^{39,40} Thus, before mixing SiCW with PP, we modified the whiskers with trimethoxy(octadecyl) silane to decrease the interfacial tension and improve the

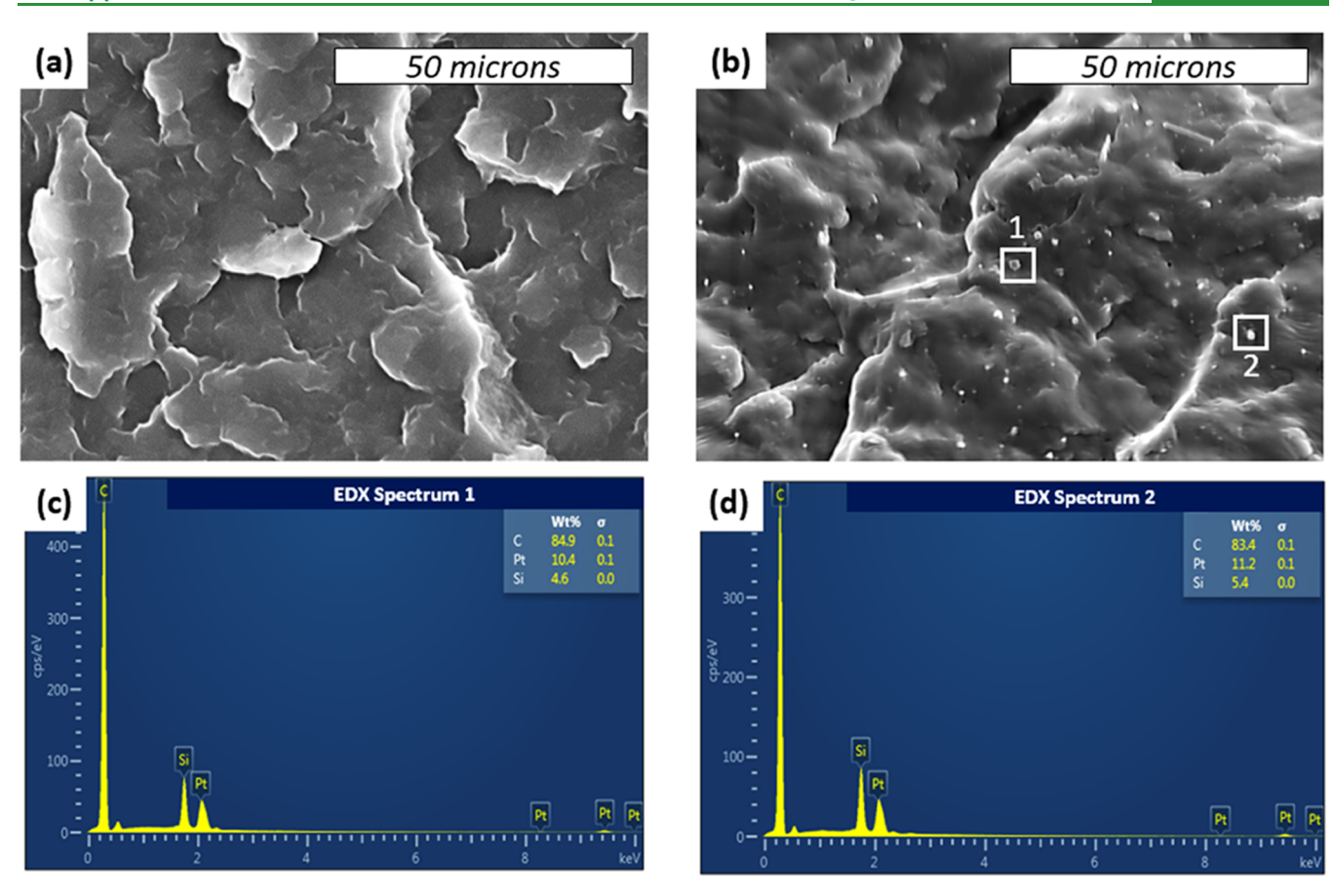


Figure 2. SEM of pure PP (a) and PP/SiCW (b) filament cross sections. Panels (c, d) are EDX spectra taken at spots 1 and 2 indicated in the image (b), respectively. Pt signal originates from platinum sputtering of the sample prior to the imaging. Therefore, the bright speckles on panel (b) correspond to SiCWs oriented in the direction of filament extrusion.

interaction between polar SiCWs and the nonpolar polymer. Following the coating step of the SiCW, silane-coated SiCWs were analyzed using TGA. The coating amount was 0.2% by weight, translated into $\sim\!0.8$ nm layer thickness. Based on the silane structure and assuming a fully extended conformation for each bond, the maximum thickness of the trimethoxy-(octadecyl) silane monolayer is $\sim\!2.3$ nm. 41 Therefore, the SiCWs were covered with either the silane monolayer in which the alkyl chains are not stretched but rather tilted to a certain degree or with incomplete monolayer. 41,42

To fabricate the composite filaments for FFF printing, we dropped the MEK/SiCW suspension over the pellets (being stirred by hand using a spatula) until the solution was exhausted and the pellets were thoroughly coated. After the solvent evaporation, PP pellets decorated with SiCWs were obtained and used for extruding the filaments (SI: S5 and Figure S4). Filament samples were prepared via cryogenic fracture to evaluate the distribution of the SiCWs in the PP matrix, and then the cross section was examined with SEM (Figure 2). The cross section of pure PP filament (Figure 2a) was compared to that of the PP/SiCW composite filaments (Figure 2b). From these images, it is evident that there is an even distribution of the SiCWs (seen as bright speckles on the SEM image) in the polymer matrix, and one can see no aggregation of the whiskers. The majority of the SiCWs appear to be oriented in the direction of the filament extrusion.

DSC results for the first heating of filaments are displayed in Figure 3. The data show that introducing SiCWs into the PP matrix has a small effect on the thermal transitions of the

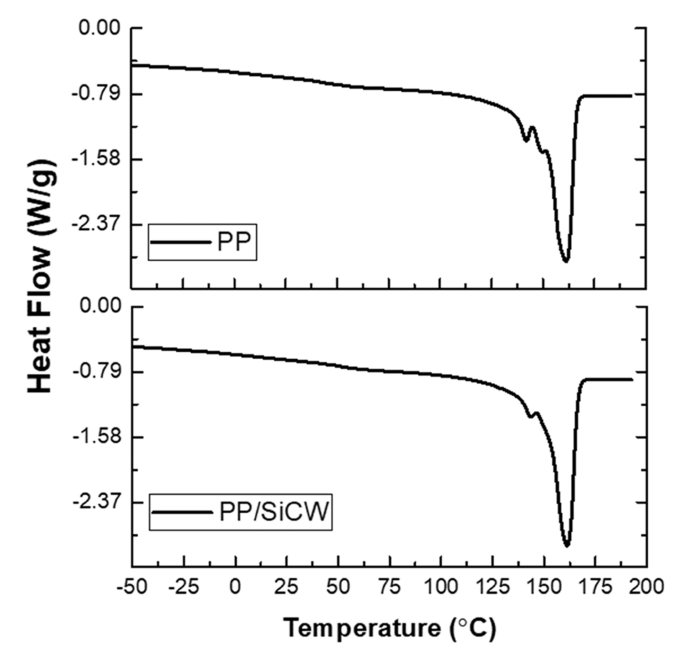
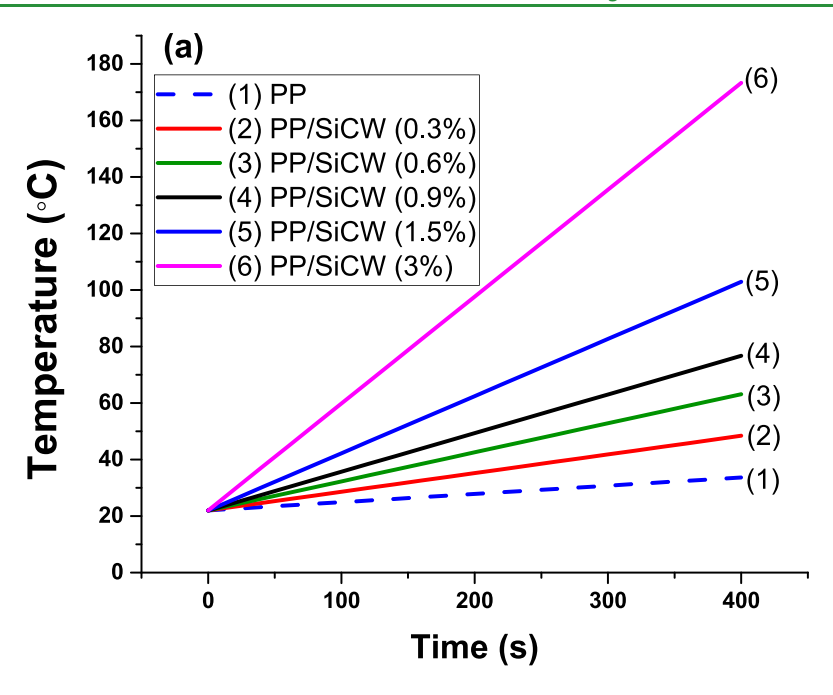


Figure 3. DSC traces for PP and PP/SiCW filaments.

polymer. The onset $T_{\rm g}$ of the PP and PP/SiCW filaments is about 0 °C. However, the observed DSC $T_{\rm g}$ region is broad and extends until ~50 °C. This broad transition can be associated with the orientation of the PP macromolecules



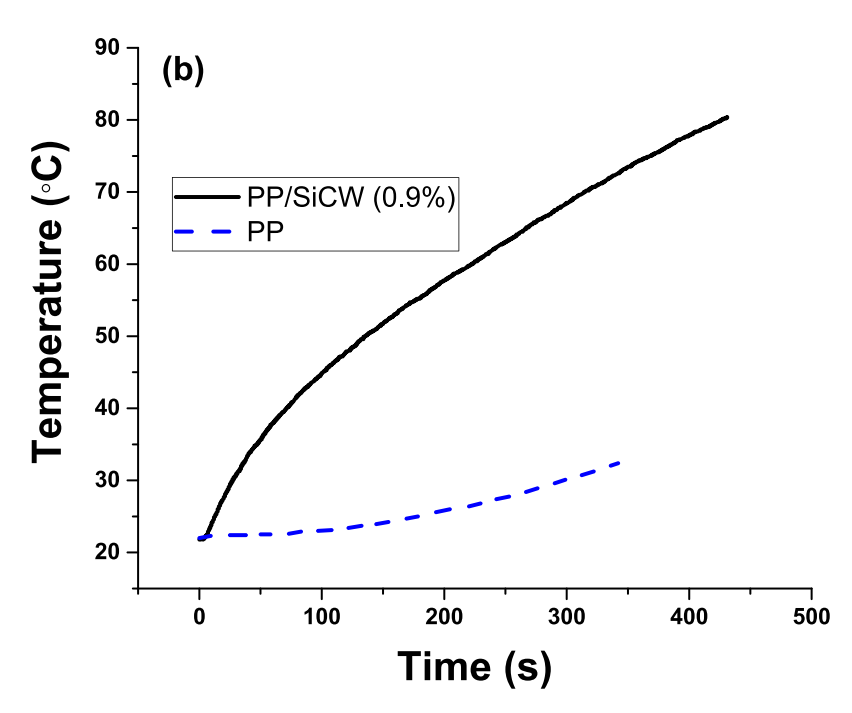


Figure 4. Temperature during MWV heating of the "temperature cubes" (a) calculated in simulations and (b) measured in experiments.

during the extrusion and the high degree of PP crystallinity. The filaments' major $T_{\rm m}$ (melting temperature) is ~164 °C, which did not noticeably change with adding SiCWs. The extruded PP-based materials also have a smaller melting peak, around 10° below the main melting peak. The main crystalline peak is typically seen in PP for α -crystals, and the lower-temperature minor peak is associated with β -crystals. The minor peak is somewhat more pronounced in the filament made from pure PP. Beyond this, we cannot observe a significant difference in percent crystallinity, as the filaments showed around the same percent of crystallinity (~40%) even after adding the inorganic additive. In general, the presence of

inorganic material in the PP matrix induces an additional nucleation and increased degree of crystallinity.³⁶ We associate the absence of the crystallinity increase with a low concentration (0.9%) of the SiCWs in the filament.

Microwave Heating of PP/SiCW-Printed Samples. To estimate the necessary amount of SiCW to be added to the PP filament, we modeled the microwave heating of the PP/SiCW mixture at different whisker contents in our 1000 Watt MWV oven. The goal was to reach a temperature well above $T_{\rm g}$ for PP to allow the macromolecules to diffuse and form entanglements. At the same time, the temperature has to be well below $T_{\rm m}$ of PP (\sim 164 $^{\circ}$ C) to avoid the change of the

sample dimensions/shape due to polymer flow. We also envision that it would be beneficial to avoid reaching $T_{\rm cr}$ (~110 °C). An additional crystallization may occur at this temperature, causing further material shrinkage and weakening the layer-to-layer bonding.

To model microwave-induced heating of PP/SiCW composites for a range of volume fractions of SiCW fillers added, we solve a heat transfer equation within the cubic composite sample coupled with the electromagnetic wave equation within the entire microwave oven. Specifically, the heat transfer equation within the sample reads

$$\rho C_{\mathbf{p}} \frac{\partial T}{\partial t} = \nabla (k \nabla T) + Q \tag{2}$$

where ρ is the density (kg/m³), C_p is the specific heat capacity at constant pressure (J/(kg·K)), k is the thermal conductivity of the sample with the chosen volume fraction of nanofillers (W/(m·K)), and Q is the volumetric heat source (W/m³) upon the application of microwave power. We assume that the composite properties are uniform on the length scale of interest. The parameters of pure PP and PP/SiCW samples are chosen based on the available literature, as detailed in Tables S3, S4, and S8. For simplicity, the material's properties are assumed to be constant during microwave heating. The volumetric heat source for the nonmagnetic material with a complex relative permittivity, $\varepsilon_r = \varepsilon_r' - j\varepsilon_r''$, is calculated based on the electric field intensity in the microwave oven, E, as 44

$$Q = \frac{1}{2}\omega\varepsilon_0\varepsilon_r''|\mathbf{E}|^2 \tag{3}$$

where ω is the angular frequency and ε_0 is vacuum permittivity. Note that for the composites with low conductivities considered herein, dielectric loss significantly exceeds conductive loss; hence, we only account for the dielectric loss in the volumetric heat source. The electric field vector ${\bf E}$ is calculated by solving the wave equation within the microwave cavity 45,46

$$\nabla \times \left(\frac{1}{\mu_{\rm r}} \nabla \times \mathbf{E}\right) - k_0^2 \varepsilon_{\rm r} \mathbf{E} = 0 \tag{4}$$

where μ_{r} is the relative permeability, $k_0 = \frac{\omega}{\epsilon_0}$ is the wave number in free space, and c_0 is the speed of light. We use COMSOL Multiphysics@ software⁴⁷ to integrate this system of equations. All simulation details are provided in Section S8 of the Supporting Information. We chose the sample size of 1 cm³ (same as in the concurrent experiments) and the exact dimensions of the microwave oven⁴⁸ used in experiments as detailed in Table S5 and SI, S8. The sample was assumed to be fully insulated in our simulations. A power of 1 kW was applied for 400 s, and the frequency $f = 2\pi/\omega$ was set in the simulations to 2.45 GHz (same as in experiments). The sample was suspended at a distance of 5 cm from the oven's bottom surface, mimicking the sample's placement at the underlying insulating foam layer in the experiments. We note that the microwave used in experiments is equipped with a mode stirrer for uniform heating. 48 The temperature within the sample as a function of time is shown in Figure 4a, where the temperature within the pure PP sample (blue dashed line) is shown along with the temperatures of the samples with different volume fractions of SiCWs (as marked in the legend); in all cases, fillers are assumed to be well dispersed in the sample. As

anticipated, the modeling shows only a moderate heating of pure PP in the oven. At sufficiently high SiCWs content (3.05% vol), the temperature reaches values well above $T_{\rm cr}$ or $T_{\rm m}$ of polypropylene within the relatively short time of MVW irradiation. Therefore, these results indicate that the optimal content of SiCWs in the PP matrix is approximately between 0.9 and 1.5% (volume % of SiCWs). In what follows, we use PP/SiCW filaments containing 0.9% vol of the whiskers in our experiments. This lower concentration was selected to minimize the influence of the added SiCWs on the properties of the PP filament.

We printed $1 \times 1 \times 1$ cm³ cubes having a hole for the temperature probe to be inserted. These "temperature cubes" were used to determine how the temperature of the printed samples changes under MWV irradiation. The results from the microwave treatment of the PP/SiCW "temperature cubes" are shown in Figure 4b. One can see that there is significant heat generated due to the presence of microwave-absorbent SiCWs in the PP matrix. Equally encouraging, these high heating levels were reached without any significant structural changes in the 3D-printed cubes. The temperature cube kept its integrity and dimensions. Our modeling approximately captures the extent of heating observed in our experiments. For instance, the temperature after 400 s was determined as 77 °C in modeling (see the black line in Figure 4a, corresponding to 0.9% vol of SiCW) and 78 °C in the experiment (shown in black in Figure 4b corresponding to the same fraction of whiskers). Hence, our modeling approach can be used in further studies to approximately predict variations in temperature in samples with various fractions of added fillers. The pronounced difference between the calculated and experimental dependencies is the nonlinearity of the one recorded in the experiment. The linear dependence of temperature on the irradiation time in Figure 4a is attributed to the fact that all of the material parameters are taken to be independent of temperature as detailed in Tables S3 and S4 and SI: S8.

Characterization of the Printed Samples. Samples from the pure PP and composite filaments were printed and used in DMA and compression testing measurements. We selected the printer bed temperature to be 40 °C to minimize the effect of the temperature on the diffusion processes during the printing and consolidation of the sample. It was the lowest (experimentally determined) temperature that allowed reliable bed adhesion during the printing of the samples. The mechanical properties of the printed structure depend on the level of contact consolidation of the printed layers. ^{49,50} For the ideal case, where the contact zone has the same properties as the bulk material, the mechanical characteristics of the obtained structures are determined by their density. The density of the printed materials depends on the area of layerto-layer contact developed via sintering. 49,51,52 It is obvious that sufficient levels of sintering are needed for the printed objects' good mechanical properties. In this work, we selected the density measurement as a parameter to evaluate the sintering extent. So, as the density of the printed samples is closer to the density of the PP bulk, the higher the level of the sintering. PP compression-molded samples were used as a reference to calculate the void fraction of the printed samples. In our calculations, we considered the presence of a small fraction of the high-density SiCWs. The results presented in Table 1 show that the samples containing SiCWs have a significantly higher level of sintering (lower pore fraction) than the pure PP-printed material. We associate this observation

Table 1. Density Measurements for the Materials and Samples' Void Fraction

sample	density (g/cm ³)	void fraction in comparison to the PP bulk
PP/SiCW	0.72	23%
PP/SiCW post MWV	0.73	21%
PP (printed)	0.66	28%
PP (bulk)	0.91	0
SiC	3.21	

with the extremely high thermal conductivity of the SiC whiskers. Thus, an increased thermal conductivity of the printed filaments allows for a longer time for samples to sinter as the lower layers are heated during the top layer application. Another important observation is that microwave treatment only slightly (\sim 2%) increases material density. Therefore, there is no significant additional sintering during the MWV irradiation. This result could be anticipated since the temperature of the samples (Figure 4b) is not approaching the melting point of the PP matrix, and the crystals restrict the flow of the material.

The DSC data for the printed samples is shown in Figure 5. The time that the filament was heated within the printing head

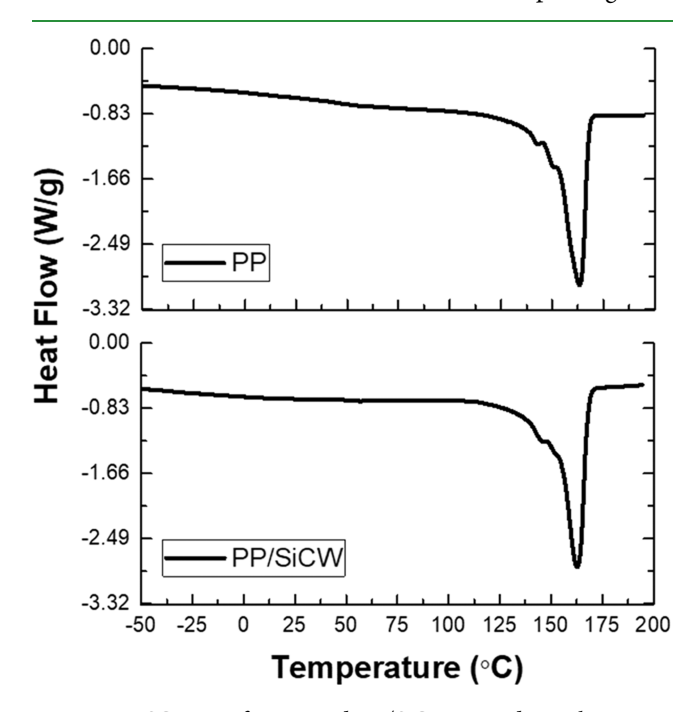


Figure 5. DSC traces for PP- and PP/SiCW-printed samples.

was relatively short, but the cooling environment was certainly different from the extrusion process used for filament fabrication. The FFF-printed parts were printed onto a heated bed and had additional heating provided by the heated nozzle swiping across the sample. First, we found that $T_{\rm m}$ is not changing significantly upon printing. The most noteworthy observation is how the printing process greatly impacts the percent crystallinity of the materials. Specifically, the percent of crystallinity for the printed samples containing SiCWs was significantly higher. If the PP-printed parts have the same degree of crystallinity as the filament used for their manufacturing (\sim 40%), PP/SiCW parts have an \sim 53% crystallinity. As for the density results, this observation can

be associated with the extremely high thermal conductivity of the SiC whiskers. The increased thermal conductivity of the printed filaments allows for longer crystallization of the lower layers heated during the top layer application. Also, the orientation of the polymer chains and SiCWs in the filament direction could cause efficient heterogeneous nucleation originating from the SiCWs' surface. We compared the crystallinity of PP/SiCW samples before and after MWV irradiation. There was no considerable difference in the degree of crystallinity since the temperature increase caused by MWV did not reach the crystallization temperature for PP (110 °C) (SI: Figure S6). Another interesting detail from the DSC results is the decrease in the lower-temperature peak associated with the β -crystals.

Estimating SiCW Effect on Mechanical Properties. We estimated the increase in modulus of the samples containing SiCWs because of reinforcing the lower modulus PP matrix with the minute amount of whiskers possessing extremely high modulus. Specifically, we calculated the modulus of PP/SiCW composites using the Halpin—Tsai model commonly used to estimate nanocomposite mechanical properties (SI: S9). ^{21,54–57} It was estimated that the possible increase in the modulus could be between 1 and 15%, depending on the orientation of the whiskers in the printed filaments. However, since the prints are produced with a 45° orientation, we expect that the highest possible modulus increase (even if all SiCWs are oriented along the printed filaments) would be around 10%, an average between 6 and 15%.

Thermomechanical Testing of the Printed Samples. DMA was utilized to record the storage modulus, the loss modulus, and the tan delta to investigate the materials' viscoelastic properties as a temperature function at low, nondestructive levels of deformation. These studies utilized a printing orientation with a \pm 45° infill, which struck a good balance between having the material oriented parallel or perpendicular to the constant strain rate. The loss modulus and tan delta results are shown in Figures 6 and 7, respectively. The data shows that the glass-transition temperature of the PP matrix is not affected by the SiCW addition and thus does not affect the storage modulus temperature dependence.

The storage modulus for the printed materials is shown in Figure 8. One can see how the addition of the SiCWs demonstrated an immediate improvement compared to that of the pure PP samples. As shown by the estimates above, this improvement cannot be attributed only to the reinforcing effect of high-modulus SiCWs. At room temperature (25 °C), PP had a storage modulus slightly below 1000 MPa, while PP/ SiCW samples had values closer to 1500 MPa. However, the greatest difference is seen when the materials are well below the glass-transition temperature for PP. Around -50 °C, the PP sample shows a storage modulus of around 1700 MPa, while the composite samples show at least 2700 MPa. While this is still not equal to what is seen in compression-molded PP samples (~4000 MPa, SI: S6 and Figure S5), we have closed the gap significantly from the unmodified PP prints. At this stage, we can also see the greatest difference between the two PP/SiCW samples, with the microwave-treated sample increasing to values above 3000 MPa.

As the DMA test runs through higher and higher temperatures, these differences greatly decrease with a loss in mechanical properties for PP, but the values for the microwave-treated samples remain somewhat higher. We associate the improvement of the mechanical properties with

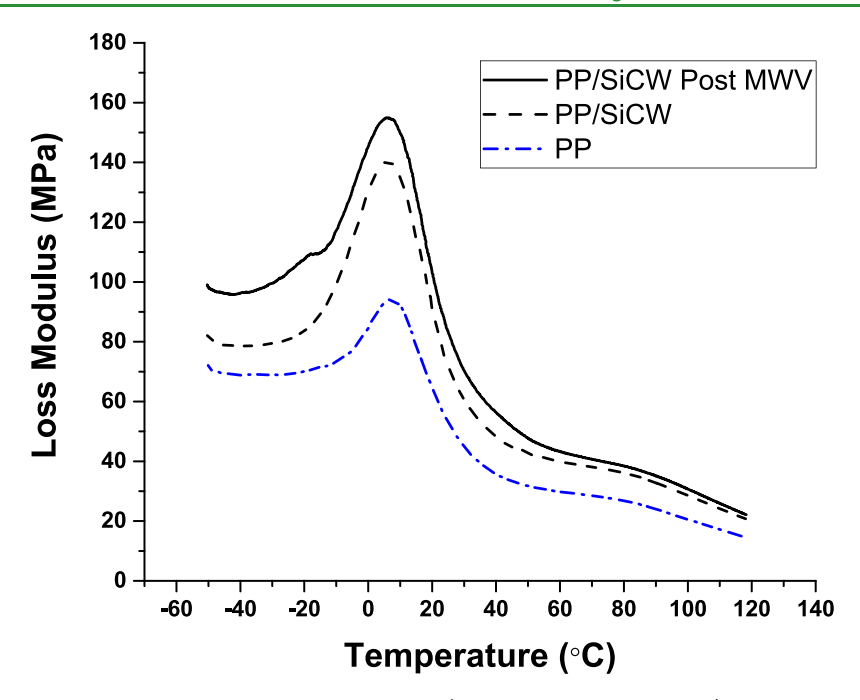


Figure 6. Loss modulus versus temperature for PP/SiCW-printed samples (untreated and MWV-treated) in comparison to that of pure PP-printed samples.

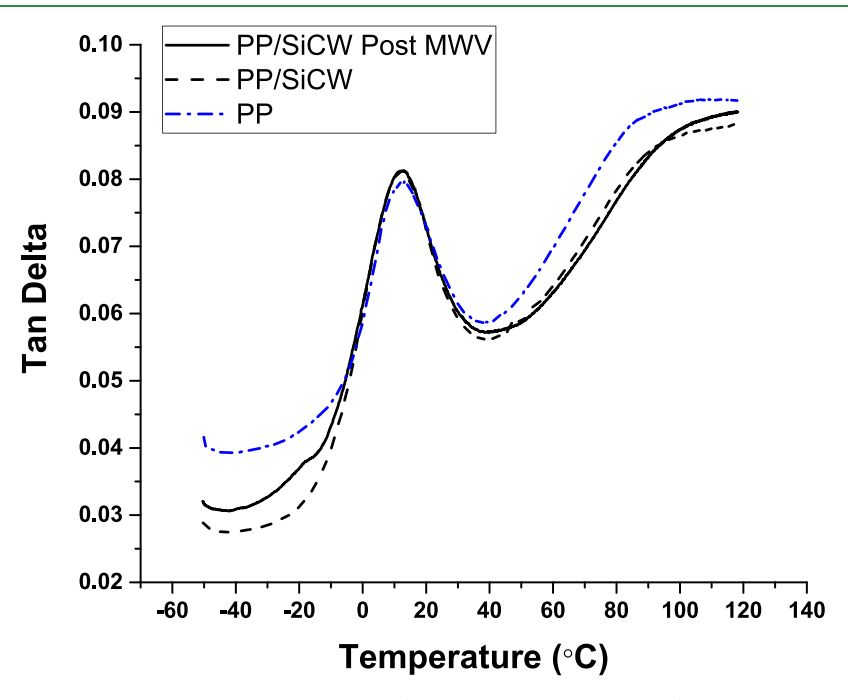


Figure 7. Tan δ versus temperature for PP/SiCW-printed samples (untreated and MWV-treated) in comparison to that of pure PP-printed samples.

an increase in the sintering level and the degree of crystallinity of the PP/SiCW samples. Since MWV treatment does not significantly change both the sintering and crystallization level for PP/SiCW-printed materials, we associate the positive effect of the MWV treatment with the integrity of the entanglement network at the weld, $\nu_{\rm W}$. Indeed, during the MWV heating of the printed samples, the temperature of the samples (Figure 4b) is significantly higher than the $T_{\rm g}$ of PP, and macromolecular segments not involved in the crystals can reorient and diffuse, increasing the level of entanglements. The effect is especially pronounced at temperatures well below $T_{\rm g}$, where

the material behaves mostly elastically, and the weld strength between the layers dictates the stress level transferred through boundaries.

Density-Adjusted Storage Modulus. To estimate the level of interfacial healing of PP/PP boundaries in the course of printing and MWV irradiation, we recalculated the storage modulus by adjusting the sample's cross section based on the porosity data (Table 1). The results are presented for 25 °C in Table 2. We considered that the strength of the welds between the printed layers reaches the maximum possible value if the adjusted storage modulus approaches the one for the PP

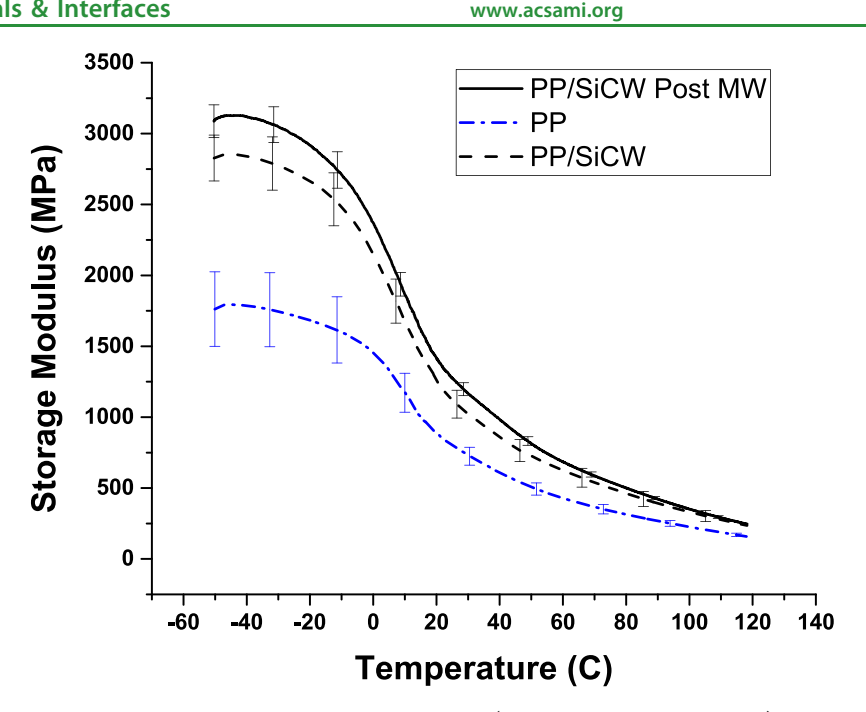


Figure 8. Storage modulus versus temperature for PP/SiCW-printed samples (untreated and MWV-treated) in comparison to that of pure PPprinted samples.

Table 2. Storage Modulus at 25 °Ca

	PP- printed	PP/SiCW	PP/SiCW Post MW	PP bulk
Storage Modulus@25 °C	811	1122	1275	
(MPa)	1038	1457	1614	1970

^aData top subrow shows data as obtained and the low subrow shows data adjusted using the porosity of the samples.

compression-molded sample. First, modulus adjustment for the PP-printed materials did not bring the modulus value close to those of the PP compression-molded samples. It is also significantly lower than the modulus of the PP/SiCW samples. The adjusted modulus for the printed PP structures is about 50% of the bulk value. Conversely, the adjusted modulus values for the PP/SiCW samples are significantly closer to the bulk ones. Remarkably, after the MWV treatment, the adjusted storage modulus of the PP/SiCW material was just ~20% lower than the PP sample obtained by compression molding. Therefore, adding SiCWs to the PP in combination with MWV irradiation considerably improves the strength of the welds between the printed layers.

Compression Testing of the Printed Structures. The printed materials' mechanical properties at a higher deformation level were studied through compression testing. For this purpose, 10 mm³ cubical samples were printed from all of the materials (SI: S5) and either treated via microwave or left untreated. Three samples were tested per set, with one set going through the microwave treatment and the other left untreated. From these tests, stress and strain graphs were built, and Young's modulus was calculated based on the slope during the linear elastic region. The representative stress-strain curves obtained are shown in Figure S7 and SI: S10. The results of the tests are displayed in Figure 9. These results showed the positive impact of the microwave treatment. The untreated PP/SiCW showed no improvement in Young's modulus compared to the pure PP samples, with Young's modulus close to 250 MPa. However, the PP/SiCW samples

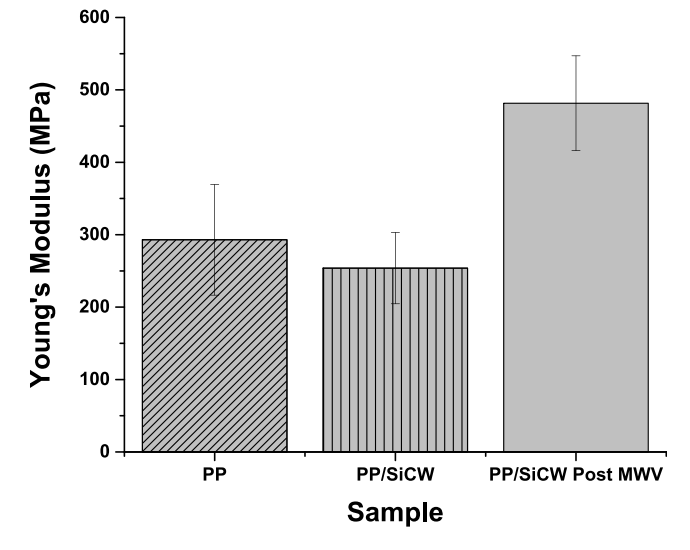


Figure 9. Young's modulus for PP/SiCW-printed samples (untreated and MWV-treated) in comparison to that of pure PP-printed samples.

improved greatly following the microwave treatment, with Young's modulus nearly twice as high as that of the untreated samples. These improvements also translated to the yield stress (Figure 10), with both PP and untreated PP/SiCW having yield stress close to 35 MPa, while the treated samples had values closer to 50 MPa.

We can also calculate the samples' toughness or ability to absorb energy during fracture based on the area under the stress and strain curves (Figure 11). The reinforced PP/SiCW sample had a toughness similar to PP (12 MJ/m²), while the microwaved samples showed significant improvement (19 MJ/ m²). The improvement in toughness shows improved strength and ductility due to improved stress transfer across the polymer layers following the additional heating provided by the MWV treatment. However, these improvements did not translate to superior yield strain (Figure 12), with the

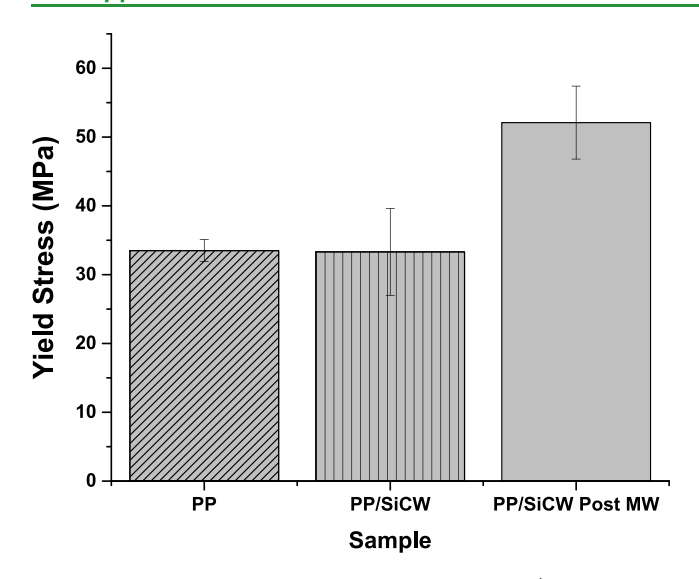


Figure 10. Yield stress for PP/SiCW-printed samples (untreated and MWV) treated in comparison to that of pure PP-printed samples.

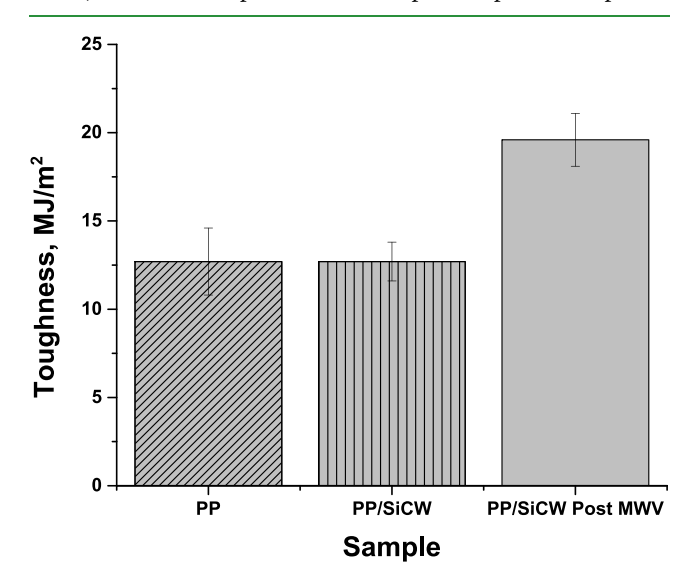


Figure 11. Toughness for PP/SiCW-printed samples (untreated and MWV-treated) in comparison to that of pure PP-printed samples.

untreated PP/SiCW samples having a strain very much in line with what we saw for regular PP-printed samples. For these values, the treated samples demonstrated a property loss because of higher modulus, with a noticeable decrease in the yield strain.

In general, because of the irradiation, Young's modulus, stress-at-yield, and toughness of the printed structures were increased by \sim 65, 53, and 55%, respectively. We noted above that the sintering and crystallization levels for PP/SiCW-printed materials do not change considerably during microwave irradiation. Therefore, the positive effect observed can be linked to improving the integrity of the entanglement network at the weld ($\nu_{\rm W}$). Due to the MWV heating, the temperature of the samples is significantly higher than the $T_{\rm g}$ of PP, and macromolecular segments not involved in the crystals can reorient and diffuse, increasing the level of entanglements. Finally, pure PP samples were treated with MWV under the same conditions and compared to untreated samples to determine how the microwave oven's environment heating influenced the final properties. Results (not shown) allowed us

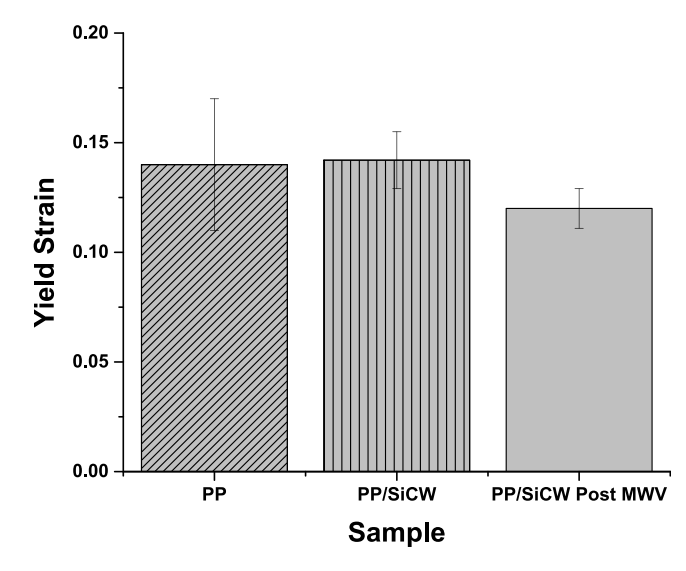


Figure 12. Yield strain of PP/SiCW-printed samples (untreated and MWV-treated) in comparison to that of pure PP-printed samples.

to conclude that the elevated chamber temperature was not high enough to influence the bulk properties of the printed part.

CONCLUSIONS

It is demonstrated that adding a minute fraction of the silanemodified SiCWs to PP filament significantly improves the mechanical and structural characteristics of the FFF-printed structures, especially with subsequent microwave treatment. The MWV irradiation (in 1000 Watt oven) causes an increase in the PP/SiCW sample temperature from room temperature to approximately 80 °C in 400 s for the samples with 0.9% vol of SiCW. This temperature is significantly higher than the $T_{\rm g}$ of PP but lower than the $T_{\rm cr}/T_{\rm m}$ of the polymer. Our modeling results show the effect of variation in the volume fraction of SiCW on the temperature increase under the MWV irradiation. The printed samples containing SiCWs have a notably higher level of sintering (lower pore fraction) and crystallinity than the pure PP-printed material. This finding can be associated with the extremely high thermal conductivity of the SiC whiskers, allowing for a longer time for samples to consolidate and crystallize as the lower layers are heated during the top layer application. It is also found that subsequent MWV treatment of the PP/SiCW structures does not substantially changes the printed material porosity and crystallinity. We attribute this result to the fact that the temperature of the samples during MWV treatment is significantly lower than the melting point of the PP matrix, and thereby the crystalline regions restrict the flow of the material.

Nevertheless, the MWV application drastically increases the mechanical characteristics of the PP/SiCW-printed materials. Namely, the adjusted (for density) storage modulus of the MWV-treated PP/SiCW material at 25 °C is just \sim 20% lower than that for the PP sample obtained by conventional compression molding. Due to the MWV irradiation, Young's modulus, yield stress, and toughness of the printed structures (measured in compression test) were increased by \sim 65, 53, and 55%, respectively. Since MWV treatment does not significantly change both the sintering and crystallization level for PP/SiCW-printed materials, we associate the positive effect of the MWV treatment with the integrity of the

entanglement network at the weld, $\nu_{\rm W}$. During the treatment, the temperature of the samples is significantly higher than the $T_{\rm g}$ of PP, and macromolecular segments not involved in the crystals can reorient and diffuse locally, increasing the level of interlayer entanglement.

ASSOCIATED CONTENT

Supporting Information

The Supporting Information is available free of charge at https://pubs.acs.org/doi/10.1021/acsami.3c07464.

Temperature profile for the FFF printing (S1); molecular weight of PP (S2); diffusion of PP macromolecules during FFF printing (S3); the radius of gyration of PP macromolecules (S4); photograph of PP/SiCW-extruded filament and printed cubical samples (S5); DMA storage modulus measurements for compression-molded PP (S6); DSC cooling curve for the extruded PP filament (S7); simulation details on modeling microwave-induced heating of pure PP and PP/SiCW samples (S8); estimating the SiCW effect on mechanical properties via the Halpin–Tsai model (S9); and representative stress–strain curves recorded in compression testing (S10) (PDF)

AUTHOR INFORMATION

Corresponding Authors

Olga Kuksenok — Department of Materials Science and Engineering, Clemson University, Clemson, South Carolina 29634, United States; orcid.org/0000-0002-1895-5206; Email: okuksen@clemson.edu

Igor Luzinov — Department of Materials Science and Engineering, Clemson University, Clemson, South Carolina 29634, United States; ⊙ orcid.org/0000-0002-1604-6519; Email: luzinov@clemson.edu

Authors

Erik L. S. Antonio – Department of Materials Science and Engineering, Clemson University, Clemson, South Carolina 29634, United States

Arefin M. Anik – Department of Materials Science and Engineering, Clemson University, Clemson, South Carolina 29634, United States

Complete contact information is available at: https://pubs.acs.org/10.1021/acsami.3c07464

Notes

The authors declare no competing financial interest.

ACKNOWLEDGMENTS

This research reported was partially supported by the National Science Foundation via EPSCoR OIA-1655740 and CBET-2134564. AMA and OK thank Dr. Yao Xiong for useful discussions of modeling microwave heating.

REFERENCES

- (1) Gross, B. C.; Erkal, J. L.; Lockwood, S. Y.; Chen, C. P.; Spence, D. M. Evaluation of 3D Printing and its Potential Impact on Biotechnology and the Chemical Sciences. *Anal. Chem.* **2014**, *86*, 3240–3253.
- (2) Hull, C. Apparatus for Production of Three-Dimensional Objects by Stereolithography. U.S. Patent US4575330.1986.

- (3) Huang, S. H.; Liu, P.; Mokasdar, A.; Hou, L. Additive Manufacturing and its Societal Impact: a Literature Review. *Int. J. Adv. Manuf. Technol.* **2013**, *67*, 1191–1203.
- (4) Prince, J. D. 3D Printing: An Industrial Revolution. *J. Electron. Resour. Med. Libr.* **2014**, *11*, 39–45.
- (5) Berman, B. 3-D printing: The New Industrial Revolution. *Bus. Horiz.* **2012**, *55*, 155–162.
- (6) Shaffer, S.; Yang, K. J.; Vargas, J.; Di Prima, M. A.; Voit, W. On Reducing Anisotropy in 3D Printed Polymers via Ionizing Radiation. *Polymer* **2014**, *55*, 5969–5979.
- (7) Ahn, S. H.; Montero, M.; Odell, D.; Roundy, S.; Wright, P. K. Anisotropic Material Properties of Fused Deposition Modeling ABS. *Rapid Prototyping J.* **2002**, *8*, 248–257.
- (8) Wang, X.; Jiang, M.; Zhou, Z. W.; Gou, J. H.; Hui, D. 3D Printing of Polymer Matrix Composites: A Review and Prospective. *Composites, Part B* **2017**, *110*, 442–458.
- (9) Bandyopadhyay, A.; Heer, B. Additive Manufacturing of Multi-Material Structures. *Mater. Sci. Eng.*, R **2018**, 129, 1–16.
- (10) Karger-Kocsis, J. *Polypropylene An A-Z Reference*; Kluwer Academic Publishers: Dordrecht, 1999; p 966.
- (11) Stoof, D.; Pickering, K. Sustainable Composite Fused Deposition Modelling Filament using Recycled Pre-Consumer Polypropylene. *Composites, Part B* **2018**, *135*, 110–118.
- (12) Carneiro, O. S.; Silva, A. F.; Gomes, R. Fused Deposition Modeling with Polypropylene. *Mater. Des.* **2015**, 83, 768–776.
- (13) Peng, X. D.; He, H.; Jia, Y. C.; Liu, H.; Geng, Y.; Huang, B.; Luo, C. Shape Memory Effect of Three-Dimensional Printed Products Based on Polypropylene/Nylon 6 Alloy. *J. Mater. Sci.* **2019**, *54*, 9235–9246.
- (14) Petersmann, S.; Spoerk-Erdely, P.; Feuchter, M.; Wieme, T.; Arbeiter, F.; Spoerk, M. Process-Induced Morphological Features in Material Extrusion-Based Additive Manufacturing of Polypropylene. *Addit. Manuf.* **2020**, *35*, No. 101384.
- (15) Gao, X.; Zhang, D. J.; Qi, S. X.; Wen, X. N.; Su, Y. L. Mechanical Properties of 3D Parts Fabricated by Fused Deposition Modeling: Effect of Various Fillers in Polylactide. *J. Appl. Polym. Sci.* **2019**, *136*, No. 47824.
- (16) Dong, M.; Zhang, S. J.; Gao, D. L.; Chou, B. G. In *The Study on Polypropylene Applied in Fused Deposition Modeling*, 34th International Conference of the Polymer-Processing-Society (PPS), Taipei, TAIWAN, May 21-25; Amer Inst Physics: Taipei, Taiwan, 2018.
- (17) Long, H. B.; Wu, Z. Q.; Dong, Q. Q.; Shen, Y. T.; Zhou, W. Y.; Luo, Y.; Zhang, C. Q.; Dong, X. M. Mechanical and Thermal Properties of Bamboo Fiber Reinforced Polypropylene/Polylactic Acid Composites for 3D Printing. *Polym. Eng. Sci.* **2019**, *59*, E247–E260.
- (18) Yuan, Z.; Yu, J.; Rao, B.; Bai, H.; Jiang, N.; Gao, J.; Lu, S. Enhanced Thermal Properties of Epoxy Composites by Using Hyperbranched Aromatic Polyamide Grafted Silicon Carbide Whiskers. *Macromol. Res.* **2014**, 22, 405–411.
- (19) Compton, B. G.; Lewis, J. A. 3D-Printing of Lightweight Cellular Composites. *Adv. Mater.* **2014**, *26*, 5930–5935.
- (20) Harris, G. L. Properties of Silicon Carbide; INSPEC, Institution of Electrical Engineers: London, 1995.
- (21) Townsend, J.; Burtovyy, R.; Aprelev, P.; Kornev, K. G.; Luzinov, I. Enhancing Mechanical and Thermal Properties of Epoxy Nanocomposites via Alignment of Magnetized SiC Whiskers. ACS Appl. Mater. Interfaces 2017, 9, 22927–22940.
- (22) Han, H. W.; Liu, H. S. Characterization of Vapour Deposited Products in Furnace Tube During SIC Synthesis from Carbonized Rice Hulls. *Ceram. Int.* **1999**, *25*, 631–637.
- (23) Luzinov, I.; Julthongpiput, D.; Liebmann-Vinson, A.; Cregger, T.; Foster, M. D.; Tsukruk, V. V. Epoxy-Terminated Self-Assembled Monolayers: Molecular Glues for Polymer Layers. *Langmuir* **2000**, *16*, 504–516.
- (24) Aïssa, B.; Tabet, N.; Nedil, M.; Therriault, D.; Rosei, F.; Nechache, R. Electromagnetic Energy Absorption Potential and Microwave Heating Capacity of SiC Thin Films in the 1-16 GHz frequency Range. *Appl. Surf. Sci.* **2012**, *258*, 5482–5485.

- (25) Mgbemena, C. O.; Li, D. N.; Lin, M. F.; Liddel, P. D.; Katnam, K. B.; Thakur, V. K.; Nezhad, H. Y. Accelerated Microwave Curing of Fibre-Reinforced Thermoset Polymer Composites for Structural Applications: A Review of Scientific Challenges. *Composites, Part A* **2018**, *115*, 88–103.
- (26) Poyraz, S.; Zhang, L.; Schroder, A.; Zhang, X. Y. Ultrafast Microwave Welding/Reinforcing Approach at the Interface of Thermoplastic Materials. *ACS Appl. Mater. Interfaces* **2015**, 7, 22469–22477.
- (27) Zhang, M.; Song, X. X.; Grove, W.; Hull, E.; Pei, Z. J.; Ning, F. D.; Cong, W. L. In *Carbon Nanotube Reinforced Fused Deposition Modeling Using Microwave Irradiation*, Proceedings of the ASME 11th International Manufacturing Science and Engineering Conference; ASME, 2016; p 7.
- (28) Sweeney, C. B.; Lackey, B. A.; Pospisil, M. J.; Achee, T. C.; Hicks, V. K.; Moran, A. G.; Teipel, B. R.; Saed, M. A.; Green, M. J. Welding of 3D-Printed Carbon Nanotube-Polymer Composites by Locally Induced Microwave Heating. *Sci. Adv.* **2017**, *3*, No. e1700262.
- (29) Wang, Y. Q.; Liu, Z. G.; Gu, H. W.; Cui, C. Z.; Hao, J. B. Improved Mechanical Properties of 3D-printed SiC/PLA composite Parts by Microwave Heating. *J. Mater. Res.* **2019**, *34*, 3412–3419.
- (30) Rostom, S.; Dadmun, M. D. Improving Heat Transfer in Fused Deposition Modeling With Graphene Enhances Inter Filament Bonding. *Polym. Chem.* **2019**, *10*, 5967–5978.
- (31) Sun, Q.; Rizvi, G. M.; Bellehumeur, C. T.; Gu, P. Effect of Processing Conditions On The Bonding Quality of FDM Polymer Filaments. *Rapid Prototyping J.* **2008**, *14*, 72–80.
- (32) Panin, S. V.; Kornienko, L. A.; Alexenko, V. O.; Buslovich, D. G.; Dontsov, Y. V. In *Extrudable Polymer-Polymer Composites Based on Ultra-High Molecular Weight Polyethylene*, 11th International Conference on Mechanics, Resource and Diagnostics of Materials and Structures (MRDMS), Ekaterinburg, RUSSIA, Dec 11-15; Amer Inst Physics: Ekaterinburg, Russia, 2017.
- (33) Levenhagen, N. P.; Dadmun, M. D. Improving Interlayer Adhesion in 3D Printing with Surface Segregating Additives: Improving the Isotropy of Acrylonitrile—Butadiene—Styrene Parts. ACS Appl. Polym. Mater. 2019, 1, 876—884.
- (34) Helfand, E.; Tagami, Y. Theory of Interface Between Immiscible Polymers. J. Polym. Sci., Part B: Polym. Lett. 1971, 9, 741–746.
- (35) Gurney, R.; Henry, A.; Schach, R.; Lindner, A.; Creton, C. Molecular Weight Dependence of Interdiffusion and Adhesion of Polymers at Short Contact Times. *Langmuir* **2017**, *33*, 1670–1678.
- (36) Sperling, L. H. Introduction to Physical Polymer Science, 4th ed.; Wiley: Hoboken, N.J, 2006; p 845.
- (37) El Moumen, A.; Tarfaoui, M.; Lafdi, K. Modelling of the Temperature and Residual Stress Fields During 3D Printing of Polymer Composites. *Int. J. Adv. Manuf. Technol.* **2019**, *104*, 1661–1676.
- (38) McIlroy, C.; Olmsted, P. D. Disentanglement Effects on Welding Behaviour of Polymer Melts During the Fused-Filament-Fabrication Method for Additive Manufacturing. *Polymer* **2017**, *123*, 376–391.
- (39) Baek, K.; Kim, H.; Shin, H.; Park, H.; Cho, M. Multiscale Study to Investigate Nanoparticle Agglomeration Effect on Electrical Conductivity of Nano-SiC Reinforced Polypropylene Matrix Composites. *Mech. Adv. Mater. Struct.* **2023**, *30*, 2442–2452.
- (40) Avella, M.; Martuscelli, E.; Raimo, M.; Partch, R.; Gangolli, S. G.; Pascucci, B. Polypropylene Reinforced with Silicon Carbide Whiskers. *J. Mater. Sci.* **1997**, 32, 2411–2416.
- (41) Wasserman, S. R.; Tao, Y. T.; Whitesides, G. M. Structure and Reactivity of Alkylsiloxane Monolayers Formed by Reaction of Alkyltrichlorosilanes on Silicon Substrates. *Langmuir* **1989**, *5*, 1074–1087
- (42) Wasserman, S. R.; Whitesides, G. M.; Tidswell, I. M.; Ocko, B. M.; Pershan, P. S.; Axe, J. D. The Structure of Self-Assembled Monolayers of Alkylsiloxanes on Silicon: A Comparison of Results From Ellipsometry and Low-Angle X-Ray Reflectivity. *J. Am. Chem. Soc.* 1989, 111, 5852–5861.

- (43) Wang, L.; Gardner, D. J. Effect of Fused Layer Modeling (FLM) Processing Parameters on Impact Strength of Cellular Polypropylene. *Polymer* **2017**, *113*, 74–80.
- (44) Rakesh, V.; Seo, Y.; Datta, A. K.; McCarthy, K. L.; McCarthy, M. J. Heat Transfer During Microwave Combination Heating: Computational Modeling and MRI Experiments. *AlChE J.* **2010**, *56*, 2468–2478.
- (45) Guru, B. S.; Hiziroglu, H. R. Electromagnetic Field Theory Fundamentals; Cambridge University Press, 2009.
- (46) Halim, S. A.; Swithenbank, J. Simulation Study of Parameters Influencing Microwave Heating of Biomass. *J. Energy Inst.* **2019**, 92, 1191–1212.
- (47) https://doc.comsol.com/5.5/doc/com.comsol.help.rf/rf_ug_radio_frequency.07.13.html. (accessed July 7, 2023).
- (48) https://www.microwaveresearch.com/BP-095.php. (accessed July 7, 2023).
- (49) Bellehumeur, C.; Li, L.; Sun, Q.; Gu, P. Modeling of Bond Formation Between Polymer Filaments in the Fused Deposition Modeling Process. *J. Manuf. Processes* **2004**, *6*, 170–178.
- (50) Wang, X.; Jiang, M.; Zhou, Z.; Gou, J.; Hui, D. 3D Printing of Polymer Matrix Composites: A Review and Prospective. *Composites, Part B* **2017**, *110*, 442–458.
- (51) Parandoush, P.; Lin, D. A Review on Additive Manufacturing of Polymer-Fiber Composites. *Compos. Struct.* **2017**, *182*, 36–53.
- (52) Bhandari, S.; Lopez-Anido, R. A.; Gardner, D. J. Enhancing the Interlayer Tensile Strength of 3D Printed Short Carbon Fiber Reinforced PETG and PLA Composites via Annealing. *Addit. Manuf.* **2019**, *30*, No. 100922.
- (53) Yun, Y. S.; Bae, Y. H.; Kim, D. H.; Lee, J. Y.; Chin, I.-J.; Jin, H.-J. Reinforcing Effects of Adding Alkylated Graphene Oxide to Polypropylene. *Carbon* **2011**, *49*, 3553–3559.
- (54) Fornes, T. D.; Paul, D. R. Modeling Properties of Nylon 6/Clay Nanocomposites Using Composite Theories. *Polymer* **2003**, *44*, 4993–5013.
- (55) Libanori, R.; Erb, R. M.; Studart, A. R. Mechanics of Platelet-Reinforced Composites Assembled Using Mechanical and Magnetic Stimuli. *ACS Appl. Mater. Interfaces* **2013**, *5*, 10794–10805.
- (56) Putz, K.; Krishnamoorti, R.; Green, P. F. The Role of Interfacial Interactions in The Dynamic Mechanical Response of Functionalized SWNT-PS Nanocomposites. *Polymer* **2007**, *48*, 3540–3545.
- (57) Nielsen, L. E. Mechanical Properties of Polymers and Composites; Dekker: New York,, 1974; Vol. 2, p 462.